Chinese Chemical Letters 31 (2020) 2583–2590

Contents lists available at ScienceDirect

Chinese Chemical Letters

journal homepage: www.elsevier.com/locate/cclet

Review

A short review on recent progress of Bi/semiconductor photocatalysts: The role of Bi metal

Qian Chen, Xuanrui Cheng, Huimin Long, Yongfang Rao*

Department of Environmental Science and Engineering, Xi' an Jiaotong University, Xi'an 710049, China

ARTICLE INFO

Article history:
Received 15 June 2020
Received in revised form 9 August 2020
Accepted 13 August 2020
Available online 15 August 2020

Keywords:
Bi metal
Plasma photocatalyst
Cocatalyst
Electron/hole trappers
Charge transfer medium

ABSTRACT

Bi/semiconductor photocatalysts have extensively been applied in the production of hydrogen, CO_2 reduction and environmental remediation in recent years. This short review summarizes the role of Bi metal as a plasma photocatalyst and cocatalyst. As a cocatalyst, Bi metal can be electron/hole trappers, charge transfer mediators, or oxygen vacancy coordinators. In addition, the preparation methods of the Bi/semiconductor photocatalysts are also reviewed. Challenges and future research directions related to Bi/semiconductor photocatalysts are discussed and summarized, including the use of advanced characterization techniques to refine the reaction mechanism, the difficulties of preparing Bi single atom catalyst, and the improvement of the reduction ability of Bi-based photocatalysts. This review helps understand the reaction mechanisms of the composite photocatalytic systems containing Bi metal and proposes new perspectives for designing the photocatalysts which can control air pollution *via* a reductive process.

1. Introduction

The ever-growing global concerns about energy crisis and environmental pollution in the past decades have encouraged the efforts to seek clean, renewable, and sustainable energy source in place of fossil fuels including coal and petroleum. Solar energy is believed as one of promising alternatives of fossil fuels due to its sustainability, abundance, easy accessibility, and environmentally friendly properties [1]. Among various methods of utilizing solar energy, photocatalytic technologies have received intensive interest in the generation of hydrogen *via* water-splitting process, the production of CH_4 *via* CO_2 reduction, and environmental remediation since the pioneering work of Fujishima *et al.* in 1972 [2].

Great efforts have been contributed to the development of semiconductor photocatalysts as the critical component of photocatalytic system. A large number of catalysts including TiO_2 [2], ZnO [3], WO_3 [4], CuS [5], $CaTiO_3$ [6], Bi_2WO_6 [7], g-C_3N_4 [8], black phosphorous [9], and perovskites [10], have been explored to use solar energy for the generation of H_2 and CH_4 and environmental pollution control. Among the explored materials, the past decade has witnessed a boost of interest in the development of bismuth-based photocatalysts due to good biocompatibility, chemical stability and narrow bandgap, most of which is below 3.0 eV. For the compounds containing Bi^{3+}, their valence bands (VBs) are believed to derive from the hybridization of O 2p and Bi $6s^2$ orbitals, leading to VBs upshift. Bismuth-based photocatalysts include bismuth oxide [11], bismuth oxyhalides [12–16], and bimetallic oxides (Bi_2WO_6, $BiVO_4$, Bi_2MoO_6, $Bi_4Ti_3O_{12}$, $BiFeO_3$, $CuBi_2O_4$, and $NaBiO_3$) [17–23]. However, the application of Bi-based photocatalysts in environmental remediation and energy conversion is not satisfactory owing to their low conduction band (CB) position and easy recombination of charge carriers. Therefore, various attempts including morphology control [19], doping [18], heterojunction construction [17,24,25], stoichiometry control [26], crystal facet control [12], defect engineering [27], and surface modification [28], have been made to increase the performance of Bi-based photocatalysts. There are a few excellent reviews regarding Bi-based photocatalysts [29–31]. However, limited review concentrated on the role of metal Bismuth in Bi-based photocatalytic systems. Bismuth metal possesses noble metal-like surface plasmon resonance (SPR) property [32]. The SPR effect of Bi can widen the light absorption range of other catalysts and promote the separation of photo-induced charge carriers when coupled with other catalysts [33]. Bi metal also has a series of other advantages, such as small effective mass, low energy band overlap, high carrier mobilities and long mean free path. In addition, Bi metal has a negative Fermi level (−0.17 eV) and a low work function (4.22 eV) [34,35]. When Bi metal is coupled with other

* Corresponding author.
E-mail address: yfrao@mail.xjtu.edu.cn (Y. Rao).

https://doi.org/10.1016/j.cclet.2020.08.018

semiconductors, the negative Fermi level and low work function help charge transfer between Bi metal and semiconductor. Considering the high cost and potential toxicity of noble metal, Bismuth has received increasing attention in the research area of photocatalysis as an ideal alternative of noble metal in recent years [23,36].

This review focuses on the possible roles of Bi metal in Bi/semiconductor photocatalysts reported in the past three years. The preparation methods of Bi coupled with Bi-based semiconductors or non-Bi-based semiconductors have been summarized. The application of Bi metal coupled with other semiconductors with and without Bi in environmental remediation and energy production has also been reviewed. We also proposed the potential research areas necessary for widespread application of these photocatalysts in water treatment, air pollution control, and clean energy generation.

2. Preparation methods

The preparation methods can determine the size, morphology, and dispersibility of Bi nanoparticles which affect the surface plasmon resonance effect and photocatalytic activity of Bi/semiconductor composite catalysts. Therefore, it is necessary to summarize the synthesis methods of Bi/semiconductor photocatalysts including Bi/non-bismuth-based material composites and Bi/bismuth-based photocatalyst composites.

2.1. Synthesis of Bi/non-bismuth-based material composites

Generally, there are generally two synthetic routes for Bi/non-bismuth-based materials: (1) Bi nanoparticles are first prepared alone and then coupled to other non-bismuth-based materials; (2) the already synthesized catalysts are mixed directly with bismuth precursors to obtain the final composites *via* a one-pot method. In the preparation of Bi metal, commonly used reducing agents include ethylene glycol, $NaBH_4$ and NaH_2PO_2. Jiang *et al.* [37] added dodecanethiol to the bismuth-containing solution at 80 °C in the absence of dissolved oxygen and moisture to form a bismuth-dodecanethiol complex. Then tri-*n*-octylphosphine was utilized to reduce the preceding complex to Bi nanoparticles. After aging, Bi nanoparticles with mean size of 12 nm were obtained. Finally, Bi/g-C_3N_4 was successfully prepared by ultrasonication in hexane and annealing at the reducing atmosphere. Li *et al.* [38] synthesized Bi nanoparticles in a water bath at 80 °C using polyvinyl pyrrolidone (PVP) as a surfactant and NaH_2PO_2 as a reducing agent. Then, tetraethyl orthosilicate ethanol solution was added to form a SiO_2 layer on the Bi nanoparticles, indicating that the Bi@SiO_2 composite was successfully prepared. Zhu *et al.* [39] first prepared the CuS catalyst by solvothermal method, and then added it to the bismuth nitrate solution containing ethylene glycol and PVP. After a hydrothermal reaction at 160 °C for 24 h, the Bi/CuS composite was successfully obtained. Feng *et al.* [40] prepared a nitrogen-doped graphene (NG)/Bi composite *via* a simple one-pot method. All solutions of NaH_2PO_2, tartaric acid, NaOH, NG and bismuth nitrate were mixed together, and then the mixture was continuously stirred at 60 °C for several hours to obtain an NG/Bi composite.

2.2. Synthesis of Bi/bismuth-based photocatalyst composites

The *in situ* reduction method is one of the most commonly used synthesis methods for Bi/bismuth-based semiconductor composites. First, the bismuth-based photocatalyst was successfully prepared, and then Bi^{3+} in the bismuth-based photocatalyst was reduced to Bi^0 by a reducing agent [41], photo irradiation [42], or H_2 [43], *etc.*, thereby forming a Bi/bismuth-based photocatalyst composite. It was also reported that the Bi/bismuth-based photocatalyst composite could be directly synthesized *via* the one-pot method. Yu *et al.* [44] successfully prepared Bi-modified Bi_2WO_6 complex by a simple *in situ* reduction method using $NaBH_4$ as reducing agent. The loading amount of Bi metal in the Bi/Bi_2WO_6 photocatalyst could be adjusted by the concentration of $NaBH_4$. The morphological characterization of the Bi/Bi_2WO_6 photocatalyst showed that the structure of Bi_2WO_6 was gradually destroyed with the increase of $NaBH_4$ concentration. Wang *et al.* [42] synthesized Bi/BiOI-Bi_2O_3 composites in methanol under ultraviolet light irradiation. Under ultraviolet light illumination, photo-generated holes were captured by methanol and Bi^{3+} produced by the partial decomposition of BiOI-Bi_2O_3 was reduced to Bi^0 by photo-generated electrons accumulated on the conduction band. Zhou *et al.* [45] successfully constructed the Bi/$Bi_2O_2CO_3$ heterojunction through the formamide-assisted one-pot method. The formamide played a dual role as a carbon/alkali source and a reducing agent. The bismuth nitrate solution and formamide were completely mixed and suffered 12 h hydrothermal treatment at 170 °C, leading to the generation of Bi/$Bi_2O_2CO_3$ composite.

3. Bi metal-based composites

3.1. Bismuth as a direct plasmonic photocatalyst

The surface electrons of the metal Bi resonate with incident photons at a suitable frequency, inducing a local electromagnetic field, which contributes to the generation and separation of hot electron-hole pairs [46–48]. The hot carriers with high energy can activate surface O_2 to produce reactive oxygen species (ROS) to participate in the subsequent redox reactions [49]. Dong *et al.* showed that the metal Bi can be used as a direct plasmonic photocatalyst for NO elimination under 280 nm light irradiation [50]. However, the isolated Bi photocatalyst has poor chemical

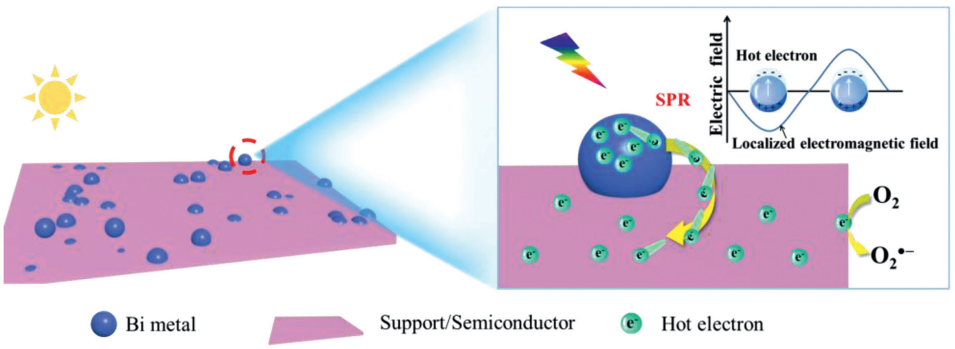

Fig. 1. Schematic diagram of the charge separation over Bi/support (semiconductor) when Bi is used as a plasma photocatalyst.

stability [51]. And the hot carriers generated *via* SPR are easily deactivated, resulting in a shortened charge transfer distance [48]. Thus, the photocatalytic performance of the metal Bi is unsatisfactory. In recent years, great endeavors have been devoted to search for suitable semiconductors or supports coupling with metal Bi to address these problems [40,49,52]. Under light irradiation, the semiconductors or supports accept the hot electrons generated by metal Bi through SPR to prevent their deactivation (Fig. 1), thereby conducing to the increased photocatalytic activity of the composites. The ideal support (semiconductor) not only facilitates the migration of hot electrons, but also improves the chemical stability of the metal Bi. Various materials have been reported as substrates for Bi loading, such as graphene oxide (GO) [53], SiO_2 [38,54] and carbon fibers [52].

Li *et al.* [49] successfully prepared uniformly dispersed Bi nanospheres using PVP surfactants, which were then loaded on GO. The numerical simulation results indicated that the electromagnetic fields generated by the adjacent Bi nanospheres superimposed to create hot carriers with high energy. The covalent interaction between Bi and GO provided a special channel for charge transport (Fig. S1a in Supporting information). The hot electrons excited by SPR tended to migrate from Bi to graphene carbon atoms, and then transferred to the carboxyl group on the edge of GO ($Bi \rightarrow C_{graphene} \rightarrow C_{COOH} \rightarrow O_{COOH}$) (Fig. S1b in Supporting information). The accumulated hot electrons can reduce O_2 to form $O_2^{\bullet-}$ to take part in the photocatalytic reaction. The introduction of GO promoted the rapid transmission of hot electrons, thus avoiding their energy loss. The prepared Bi-NPs@GO exhibited excellent photocatalytic activity in terms of NO elimination. In addition, Bi@graphene nanocomposite also possessed good photocatalytic disinfection activity for *Escherichia coli (E. coli)* under UV light irradiation [55]. This is attributed to the SPR effect of the metal Bi and the effective separation of carriers promoted by GO. The H_2O and O_2 molecules on the photocatalyst surface were activated to form ROS with strong oxidizing ability, which can directly kill bacteria. It has been reported that a thin SiO_2 shell enhanced the stability of Bi, while its activity was not affected [38]. The porous SiO_2 shell can not only be used as a protective layer to inhibit the oxidation of the active Bi core, but also as a specific transmission channel to promote the separation of hot carriers. The photocatalytic activities of Bi@SiO_2 with different molar ratios (Bi:SiO_2 = 1:0.1, marked as S1; Bi:SiO_2 = 1:0.3, marked as S2) were compared with those of pure Bi and SiO_2. The results showed that the removal efficiency of both Bi@SiO_2 composites and pure Bi achieved 100% for rhodamine B (RhB, solution pH 3) (Fig. S2a in Supporting information). In bisphenol A (BPA) solution (pH 7), the Bi@SiO_2 composites displayed significantly improved degradation efficiency (70%) of BPA compared to Bi (12%) (Fig. S2b in Supporting information). Chen *et al.* [48] constructed Bi-$BiPO_4$ nanocomposite by *in situ* solvothermal reduction method, and the removal efficiency for NO (initial concentration: ~400 ppb) reached 32.8% over Bi-$BiPO_4$ nanocomposite under visible light irradiation for 30 min. The generated hot electrons migrated from Bi to $BiPO_4$ through the Bi-$BiPO_4$ interface, facilitating the valid separation of hot carriers. The calculation manifested that compared with $BiPO_4$ top and Bi top, O_2 and NO molecules were more easily activated at the Bi-$BiPO_4$ interface, which contributed to the succedent photocatalytic reaction.

The metal Bi possesses a series of unique advantages, such as negative Fermi level (−0.17 eV) [34], relatively low work function (~4.22 eV) compared to most metals [56], and less energy level overlap between the VB and the CB. When the size of Bi is reduced to the nanoscale, the unique nano-quantum confinement will induce the transition of Bi from metal to semiconductor [57]. Thus, after Bi is coupled to the semiconductor with a matching band gap structure, the electrons generated in Bi tend to transfer to the CB of the semiconductor under light irradiation. This effectively promotes the spatial separation of electron-hole pairs, resulting in significant photocatalytic performance. Jiao *et al.* [58] systematically explored the charge transfer mechanism in the Bi/TiO_2 heterojunction under visible light irradiation by using the *in situ* XPS method (Fig. S3a in Supporting information). The results showed that the electrons generated by the SPR effect of Bi firstly migrated to the CB of TiO_2 and then transferred to the outer Bi_2O_3 layer of Bi. Meanwhile, in the outmost Bi_2O_3 layer, the immigrant electrons can reduce Bi_2O_3 to elemental Bi (Fig. S3b in Supporting information). The TiO_2 acted as a "charge transfer bridge". This special charge transfer route was attributed to the fact that the Fermi level of Bi is lower than that of n-type TiO_2 and higher than that of p-type Bi_2O_3. The layered 2D/2D heterojunction Bi@Bi_5O_7I/rGO composite was constructed by Liang *et al.* [34], displaying the large contact area and abundant charge transmission channels. The photocatalytic degradation efficiency of levofloxacin (LVFX, 20 mg/L) over Bi@Bi_5O_7I/rGO ternary composite achieved 87.7% under visible light irradiation ($\lambda > 420$ nm). The addition of Bi strengthened the light absorption of the catalyst in the visible region. The hot electrons excited on the Bi surface easily migrated to the conduction band of Bi_5O_7I, since the latter's conduction band position was lower than the former's Fermi level. The accumulative photogenerated electrons on the Bi_5O_7I continued to flow into the rGO nanosheets, leading to rapid charge transfer in the entire system.

A bifunctional Bi/α-$FeC_2O_4{\cdot}2H_2O$ (Bi/α-FOD) composite was reported to exhibit excellent visible light-driven photoreduction activity for Cr (VI) and high Fenton oxidation activity for RhB decompostion [57]. In the Bi/α-FOD system, the electrons excited by SPR migrated from Bi to the conduction band of α-FOD, and the electrons inspired on the valence band of α-FOD maintained the initial state of Bi, significantly inhibiting the recombination of photogenerated carriers. Furthermore, the formed Fe(III) can be reduced by Bi to prevent the decomposition of α-FOD. The accumulated electrons on the conduction band of α-FOD completely reduced Cr(VI) to Cr(III), and the $^{\bullet}OH$ produced by Fenton reaction effectively degraded RhB. He *et al.* [59] activated amorphous Bi_2WO_6 by depositing Bi_2O_3 and Bi in order on its surface. Since the Fermi level of Bi was higher than the conduction band of Bi_2O_3 and Bi_2WO_6, the migration direction of photoexcited electrons was: Bi → Bi_2O_3 (CB) → Bi_2WO_6 (CB). The photoexcited holes were transferred directly from the VB of Bi_2WO_6 to the VB of Bi_2O_3, showing prominent charge separation. The photocatalytic efficiency of Bi/Bi_2O_3/Bi_2WO_6 ternary heterojunction for NO removal was increased, which was ascribed to the synergistic effect of heterojunction structure and SPR.

In short, the generation of hot electrons through the SPR effect of Bi can activate surface oxygen molecules to produce a large number of reactive oxygen species. Bi transfers from metal to semiconductor when the size of Bi particles is reduced to the quantum scale. Therefore, the metal Bi can act as a plasma photocatalyst, and related reports are listed in Table S1 (Supporting information).

3.2. Bismuth as electron or hole trapper

In addition to the role as a plasma photocatalyst, the metal Bi can also play the role of the cocatalyst when coupled with other semiconductors [60]. In general, Bi can be used as an electron acceptor or hole trap to reduce the recombination of photogenerated carriers in semiconductors, leading to the increased photocatalytic activity of the semiconductors. Wang *et al.* [61] boosted the photocatalytic degradation efficiency of ciprofloxacin (CIP) by using zero-dimension (0D) Bi nanodots as charge gathering regions. The degradation rate of CIP over 0D Bi/2D

Bi_3NbO_7 was 4.58 times higher than that over pure Bi_3NbO_7 (Fig. S4a in Supporting information). And Bi/Bi_3NbO_7 showed enhanced mineralization ability for the removal of antibiotics. Since the conduction band (−0.49 eV) of Bi_3NbO_7 is more negative than the Fermi level of Bi, the Bi can continuously receive photogenerated electrons from the CB of the Bi_3NbO_7, thereby promoting the separation of photoexcited carriers in the Bi_3NbO_7 semiconductor. The formation of strong covalent bond between Bi atoms in Bi nanodots and Bi-O layer in Bi_3NbO_7 provided transport channels for charge migration. Meanwhile, molecular oxygen adsorbed on Bi captured the accepted electrons to produce $O_2^{\bullet-}$, and then further formed singlet oxygen ($^1O_2$) (Fig. S4b in Supporting information). The radical trapping experiments confirmed that these active species played an important role in the photocatalytic degradation of CIP over Bi/Bi_3NbO_7. Jia *et al.* prepared the flower-like Bi/Bi_2WO_6 microspheres [62], displaying high photocatalytic activity in terms of the removal of phenol and Cr(VI) under visible light irradiation. Due to the different work functions of Bi and Bi_2WO_6, electrons tended to transfer from Bi to Bi_2WO_6 until the Fermi level reached equilibrium. Thus, an anti-barrier layer was built at the Bi/Bi_2WO_6 interface, which accelerated the photoinduced carrier migration. The photogenerated electrons on the CB of Bi_2WO_6 were quickly transferred to the Bi surface due to the built-in electric field at the interface. The electrons accumulating on Bi surface activated molecular oxygen to generate active oxygen species to eliminate pollutants.

Sun *et al.* [60] *in situ* deposited Bi nanoparticles on the surface of $Bi_2O_2CO_3$ nanoplates (marked as BBOC) by a new method without the addition of reducing agents. The prepared BBOC composites were applied for photocatalytic hydrogen production. In 100 mL of an alkaline solution, the BBOC composite (50 mg dosage) could produce 244.5 μmol/g of H_2 after 3 h under simulated sunlight. The hydrogen production rate over BBOC (81.5 $\mu mol\ g^{-1}\ h^{-1}$) was 2 times faster than that over pure $Bi_2O_2CO_3$ (41.1 $\mu mol\ g^{-1}\ h^{-1}$). The enhanced photocatalytic activity of BBOC was attributed to Bi receiving photogenerated electrons from $Bi_2O_2CO_3$, which promoted the efficient separation of photogenerated electron-hole pairs. This helped to increase the quantum yield of photolyzing water to produce hydrogen over BBOC. In recent years, the studies about Bi as an electron capture center have been widely reported, such as Bi QDs/$Bi_4V_2O_{11}$ [63], Bi/Bi_2WO_6 [64], BiO_{2-x}/Bi [65] and $Bi/g\text{-}C_3N_4$ [37].

A limited number of articles suggest that Bi can also be used as a hole trapping center, thereby increasing the reducing capacity of the reaction system. In the Bi/TiO_2 heterojunction [56], the quantum confinement effect of Bi quantum dots endows it with semiconductor properties, which offers Bi the ability to trap holes. The high-resolution XPS spectra of Bi 4f showed that the ratio of Bi^{3+}/Bi^0 increased from 1.314:1 to 2.986:1 as the illumination time increases (Fig. S5a in Supporting information). This may be because Bi quantum dots were gradually oxidized to Bi^{3+} after capturing photogenerated holes. Therefore, Bi quantum dots consumed photogenerated holes under visible light irradiation, thereby promoting the effective separation of photoexcited carriers. The photogenerated electrons remaining on the CB of TiO_2 participated in the photocatalytic reduction reaction. For bromate which is a carcinogenic disinfection by-product, the Bi/TiO_2 heterojunction exhibited excellent photocatalytic reduction activity without the addition of sacrificial agents. After 60 min of the reaction, the bromate concentration decreased to 0, and bromide was the only reaction product (Fig. S5b in Supporting information), indicating that the bromate can be completely removed in the Bi/TiO_2 system. To date, the studies about Bi as a hole trapping/consumption center are very limited. The improvement of the reduction performance in the photocatalytic system containing Bi metal needs further investigation.

3.3. Bismuth as charge transfer medium

The Bi can be employed as a charge transfer medium between different semiconductors because it possesses good conductivity [66]. When Bi is coupled with semiconductors, Bi can transfer photoinduced electrons from one semiconductor conduction band to another semiconductor conduction band as a charge mediator, as shown in Fig. 2a. The presence of Bi accelerates the migration speed of photogenerated charges, thereby significantly increasing the removal efficiency of pollutants, as shown in the photocatalytic systems of CdS QDs/Bi/Bi_2WO_6 [67], $Bi/\alpha\text{-}Bi_2O_3/g\text{-}C_3N_4$ [68] and $Bi_2MoO_6/Bi/TiO_2$ [69]. Moreover, the introduction of Bi can also constitute an all-solid-sate Z-Scheme heterojunction (Fig. 2b). The Z-Scheme migration mechanism of carriers not only facilitates the spatial separation of photoexcited electron-hole pairs, but also retains strong redox capacity [17]. Xu *et al.* [23] constructed a ternary $Cu_2O/Bi/Bi_2MoO_6$ Z-Scheme heterojunction system by combining Bi spheres with Cu_2O/Bi_2MoO_6 hollow spheres. The removal efficiency of sulfadiazine (SDZ) and Ni(II) reached 98.6% and 93.2% after 100 min and 60 min over this composite under visible light irradiation, respectively. In a mixed system containing organic pollutants and heavy metal ions, the $Cu_2O/Bi/Bi_2MoO_6$ Z-scheme heterojunction removed both contaminants at the same time, and exhibited superior photocatalytic performance compared to Bi_2MoO_6. The significant increase of photocatalytic activity was ascribed to the effective divorcement of photogenerated carriers in the ternary system. In detail, the photoinduced electrons on the conduction band of Bi_2MoO_6 easily migrated to Bi. The strengthened electric field around the Bi spheres facilitated the continuous migration of electrons to the valence band of Cu_2O, and then recombined with photoinduced holes. In the carrier transmission pathway of the ternary $Cu_2O/Bi/Bi_2MoO_6$ composite, Bi played a role of an electronic medium. Deng *et al.* [66] synthesized graphene-functionalized Z-scheme heterojunction through utilizing Bi as a bridge to connect BiOCl and Bi_2O_3. This multi-component system showed the highest photocatalytic activity (99.7%) under visible light in terms of 2-nitrophenol removal. The synergistic effect of multi-channel charge transport (Bi-bridge and rGO) and efficient charge separation was the key for the increased activity. The photoexcited electrons generated by Bi_2O_3 were transferred to the valence band of BiOCl with oxygen vacancies through the Bi-bridge. The holes with strong oxidizing capability remaining on Bi_2O_3 can oxidize 2-nitrophenol. The removal efficiency of chemical oxygen demand (COD) in actual industrial wastewater reached 70.3% with the addition of 1 mL 30% H_2O_2 in BiOCl-Bi-Bi_2O_3/rGO system under visible light for 11 h. In the heterojunction structure containing Bi, Bi plays the part of charge transport bridges. The similar carrier migration mechanisms have also been reported in other systems, such as Bi-Bi_2MoO_6 nanosheet/CdS-diethylenetriamine [70], $Bi/BiPO_4/Bi_2WO_6$ [71] and Bi-BiOCl/AgCl [72]. The Bi metal has the

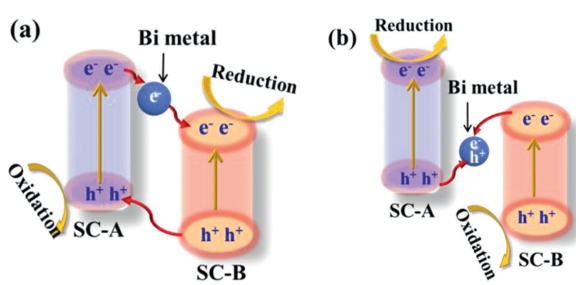

Fig. 2. The mechanism diagram of Bi metal as a charge transfer medium in type-II heterojunction (a) and all-solid Z-scheme heterojunction (b), respectively.

potential of replacing precious metals as a charge transport channel to enhance separation efficiency of electron-hole pairs.

Besides serving as an electronic medium between different semiconductors, Bi was also reported to play a role in transferring charge at the interface of layered semiconductors. Xu *et al.* [73] compared the charge transport mechanism of Bi deposited on different exposed crystal planes of Bi_2MoO_6. The structure of Bi_2MoO_6 consists of $Bi_2O_2^{2+}$ units and MoO_4^{2-} slabs, and the internal electric field region can be established between the layers. The charge alternation directions of the (001) and (010) crystal planes of Bi_2MoO_6 are completely different. The results indicated that Bi deposited on the (001) facet forms strong covalent interactions with O in both $Bi_2O_2^{2+}$ and MoO_4^{2-}, facilitating interfacial charge transmission. Based on theoretical calculations and experiments, two charge transport channels for Bi deposition on the (001) and (010) facets of Bi_2MoO_6 were proposed (Figs. 3a and b). The charge in Bi-BMO-001 was transferred through the $Bi_2O_2^{2+} \rightarrow Bi \rightarrow MoO_4^{2-}$ channel (Fig. 3a). This efficient migration channel prolonged the lifetime of electrons and dramatically increased the separation efficiency of photogenerated electron-hole pairs. On the other hand, the bulk charge alternation in Bi-BMO-010 promoted carrier recombination. Even though Bi can trap electrons, the weak interactions between layers hindered the charge migration. For Bi_2MoO_6 on the exposed (001) facet, the incorporation of Bi greatly enhanced the photocatalytic performance. Compared with that over BMO-001, the removal efficiency of sodium pentachlorophenate (NaPCP) over Bi-BMO-001 increased 2.9 times under visible light irradiation. The photocatalytic activity of Bi-BMO-010 only ascended 0.9 times (Fig. 3c). This unique charge transport channel of $Bi_2O_2^{2+} \rightarrow Bi \rightarrow MoO_4^{2-}$ and the electronic localization induced by Bi accelerated the charge delivery to molecule oxygen. As a result, Bi-BMO-001 could generate a large number of $O_2^{\bullet-}$ and $^1O_2$ radicals (Fig. 3d), suggesting the rapid interfacial charge migration could effectively activate the molecular oxygen.

The similar electron transport pathway was proposed in the work of Li *et al.* [74]. The charge migration along the $Bi_2O_2^{2+} \rightarrow Bi \rightarrow Br^-$ route at the Bi-BiOBr-010 interface resulted in the interfacial charge separation. The Bi-BiOBr-010 composite constructed by depositing Bi on the exposed (010) plane of BiOBr presented increased NO removal efficiency (60.4%) compared to BiOBr-010 (14%). After five cycling tests, the removal efficiency of NO over Bi-BiOBr-010 remained at the initial level without significant inactivation, indicating good stability and persistence. A new route of charge migration along surface cation → plasmonic metal → anion was established in the plasmonic photocatalysts. When charge alternation occurs on the exposed crystal planes of the photocatalysts, this particular pathway facilitates the interfacial charges separation, markedly increasing the photocatalytic efficiency. The design of photocatalysts by coupling plasmonic metals to specific crystal surfaces will be a promising research area.

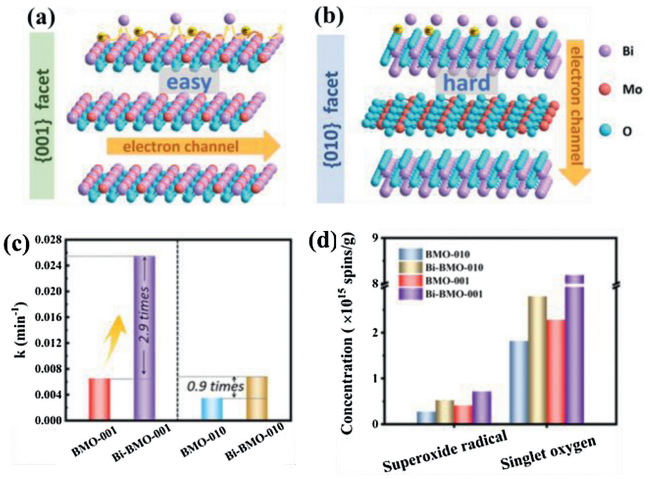

Fig. 3. Schematic diagram of the interface charge migration pathways over $Bi@Bi_2MoO_6$ on the (001) facet (a) and (010) facet (b). (c) The degradation rate constants of NaPCP over Bi_2MoO_6 and $Bi@Bi_2MoO_6$ at different exposed crystal surfaces. (d) $O_2^{\bullet-}$ and $^1O_2$ concentration detected by ESR in different photocatalysts. Reprinted with permission [73]. Copyright 2020, American Chemical Society.

Overall, metal Bi plays a role of cocatalyst in the composites, where it can trap electrons/hole or act as a charge transfer medium. Table 1 [37,39,43,60,63–65,67–71,75–86] lists the applications of Bi as a cocatalyst for the degradation of pollutant and energy production.

3.4. Synergistic effect of Bi metal and oxygen vacancies

In general, Bi/semiconductor composites [58] are usually prepared by *in situ* reduction of bismuth-based photocatalysts. The composites constructed by this method are often accompanied by the generation of oxygen vacancies [87–89]. The introduction of oxygen vacancies (OVs) can improve the activity of photocatalysis effectively, which is attributed to the defect energy levels formed between the CBs and VBs [90,91]. However, the deactivation of oxygen vacancies weakened the photocatalytic activity during the cyclic use of photocatalyst [92]. Chen *et al.* [93] prepared Bi metal-loaded $Bi_2O_2CO_3$ (Bi@OV-BOC) to improve the stability of OVs. The existence of OVs was proved by EPR. Oxygen vacancies in the Bi@OV-BOC were more stable than in OV-BOC (Fig. S6a in Supporting information). The existence of Bi metal nanoparticles improved the stability of OVs by capturing O_2 and H_2O molecules which were able to occupy the oxygen vacancies. The total charge (Δq) of O_2 calculated by density functional theory (DFT) followed the order: BOC (0.14 e) < OV-BOC (−0.076 e) < Bi@OV-BOC (−0.39 e), indicating that the presence of Bi metal was favorable for the O_2 activation to generate ROS. The transfer path of e^- in Bi@OV-BOC was: $e^- \rightarrow$ OVs → Bi → O_2, which contributed to restraining the recombination of photogenerated charge carriers. In addition, the bond length of O_2 adsorbed on the surface of Bi@OV-BOC was maximum (Fig. S6b in Supporting information), indicating that Bi metal nanoparticles contributed to the activation of O_2 molecules as well. The photocatalytic activity of Bi@OV-BOC was tested by eliminating NO. The removal ratio of NO over Bi@OV-BOC reached 40.8%. It still maintained high photocatalytic activity (34.5%) after five cycles of experiments.

The existence of Bi can not only inhibit the deactivation of OVs, but also compose the charge transfer channel with OVs to promote the separation of photogenerated carriers, leading to the generation of more ROS and increased photocatalytic activity. In addition, the SPR effect of Bi induces the generation of hot electrons to increase the quantum yield. Cui *et al.* [94] successfully deposited Bi on the surface of Bi_3O_4Cl with OVs. The results showed that the deposition amount of Bi was positively correlated with the amount of OVs. The introduction of Bi metal was conducive to the formation of OVs. The charge difference distribution reveals that Bi metals serve as the charge transfer channel and yield hot electrons which was transferred to the conduction bands of Bi_3O_4Cl. As a result, the separation of photogenerated carriers and the production of ROS were promoted. With the increase of Bi amount, the removal ratio of NO increased first and then slightly decreased. The NO removal ratio over the optimal photocatalyst was 36.78%. Besides, some researchers reported the same mechanism that Bi metals and OVs co-served as charge transfer channels. Dong *et al.* [95] prepared Bi metal@defective BiOBr. Under the visible light irradiation ($\lambda > 420$ nm), 0.20 g of the optimal photocatalyst removed 63.53% NO. Wang *et al.* [96] constructed Bi

Table 1
The bismuth acts as a co-catalyst in order to transfer or trap charges.

Photocatalysts	Preparation	Reactants	Reaction conditions	Photocatalytic efficiency	Ref
Bi/g-C_3N_4	–	NO: 500 ppb	Photocatalyst: 0.2 g; Light source: visible light (> 420 nm); Irradiation time: 30 min	60.8%	[37]
CdS QDs/Bi/Bi_2WO_6	*In situ* reduction and deposition process	RhB: 10 mg/L Formaldehyde: 6.6 mg/L	Photocatalyst: 1 g/L (RhB), 0.3 g (formaldehyde); Light source: visible light (> 420 nm); Irradiation time: 120 min (RhB), 3 h (formaldehyde)	RhB: 95.5% Formaldehyde: 75%	[67]
Bi/$Bi_4O_5I_2$	One-pot solvothermal method	bisphenol A: 20 mg/L methyl orange: 20 mg/L	Photocatalyst: 1 g/L; Light source: visible light (> 420 nm); Irradiation time: 15 min (BPA), 50 min (MO)	BPA: 94% MO: 99.4%	[75]
Bi/$BiVO_4$/V_2O_5	Annealing of $BiVO_4$ in Ar/H_2	O_2 evolution	Photocatalyst: 40 mg; Light source: visible light (> 400 nm); Irradiation time: 20 min	2413 μmol g^{-1} h^{-1}	[43]
Bi-BiOI	Hydrothermal	BPA: 10 mg/L MB: 10 mg/L	Photocatalyst: 1 g/L; Light source: visible light; Irradiation time: 4 h (BPA), 120 min (MB)	BPA: 86% MB:80%	[76]
Bi-Bi_2MoO_6/CdS-DETA	Solvothermal	H_2 evolution	Photocatalyst: 50 mg; Light source: visible light (> 420 nm)	7.37 μmol h^{-1} g^{-1}	[70]
Bi/α-Bi_2O_3/g-C_3N_4	Calcination-photoreduction technique	TC: 10 mg/L RhB: 5 mg/L	Photocatalyst: 1 g/L; Light source: visible light (> 400 nm); Irradiation time: 180 min (TC), 90 min (RhB)	TC: 90.2% RhB: 95.6%	[68]
Bi/$BiPO_4$/Bi_2WO_6	One-step solvothermal method	MB: 10 mg/L 2,4-Dichlorophenol: 30 mg/L	Photocatalyst: 1 g/L; Light source: Xenon lamp; Irradiation time: 75 min	MB: 62% 2,4-Dichlorophenol: 0.0118 min^{-1}	[71]
BiO_{2-x}/Bi	Time-dependent method	BPA: 20 mg/L	Photocatalyst: 1 g/L; Light source: visible light (> 420 nm); Irradiation time: 300 min	83.0%	[65]
Bi/Bi_5O_7Br-OV	Hydrothermal	Phenol: 10 mg/L	Photocatalyst: 0.1 g/L; Light source: visible light (> 420 nm); Irradiation time: 120 min	99%	[77]
Bi/Bi_2WO_6	Solvothermal	NO: 600 ppb	Photocatalyst: 0.3 g; Light source: visible light (> 400 nm); Irradiation time: 35 min	53.1%	[64]
Bi-Bi_2MoO_6/TiO_{2-x}	Hydrothermal and *in situ* solid-state chemical reduction	Phenol: 10 mg/L Oxygen evolution	Photocatalyst: 1 g/L(phenol), 3 g/L (oxygen evolution); Light source: visible light (> 420 nm); Irradiation time: 210 min (phenol)	Phenol: 95% oxygen evolution: 134 μmol h^{-1} g^{-1}	[69]
Bi QDs/$Bi_4V_2O_{11}$	Two-step hydrothermal	CO_2 photoreduction	Photocatalyst: 0.10 g; Light source: Xenon lamp	3.24 μmol g^{-1} h^{-1}	[63]
Bi/BiOBr	Combustion method	RhB: 10 mg/L	Photocatalyst: 1 g/L; Light source: Visible light; Irradiation time: 30 min	95.2%	[78]
Bi-$Bi_{12}O_{17}Cl_2$	*In-situ* chemical reduction	RhB: 20 mg/L TC: 15 mg/L BA: 1 mol/mL	Photocatalyst: 1 g/L (RhB,TC), 10 g/L (BA); Light source: visible light (400−780 nm); Irradiation time: 150 min (RhB/TC), 8 h (BA)	RhB: almost complete degradation BA :45%	[79]
rGO QDs-Bi-Bi_2WO_6/EP	liquid-phase deposition method	RhB: 20 mg/L Phenol: 20 mg/L	Photocatalyst: 1 g/L; Light source: visible light (>420 nm); Irradiation time: 15 min (RhB), 75 min (phenol)	RhB: 95% Phenol: 93%	[80]
g-C_3N_4@Bi/BiOBr	Solvothermal	TC: 12 mg/L RhB: 20 mg/L	Photocatalyst: 1 g/L; Light source: visible light; Irradiation time: 80 min (RhB), 4 h (TC)	RhB: 98% TC: 78%	[81]
WO_{3-x}/Bi/BiOCl	Solvothermal	RhB: 10 mg/L	Photocatalyst: 0.05 g; Light source: Vis/NIR/UV light; Irradiation time: visible light (3 min) / NIR (120 min) / UV (8 min) light	Vis: 100% NIR: 96% UV: 100%	[82]
Bi-BiO	Partial reduction with $NaBH_4$	NO: 500 ppb	Photocatalyst: 0.20 g; Light source: visible light (> 420 nm); Irradiation time: 30 min	53.0%	[83]
BiOI/Bi/Bi_2S_3	Hydrothermal	RhB: 20 mg/L	Photocatalyst: 0.2 g/L; Light source: visible light (> 420 nm); Irradiation time: 30 min	90%	[84]
Bi/Bi_5O_7I/Sn_3O_4	–	H_2 evolution	Photocatalyst: 50 mg; Light source: visible light (> 400 nm); Irradiation time: 5 h	1630 μmol/g	[85]
Bi/CuS	Two-step hydrothermal method	MB: 1×10^{-5} mol/L MO: 1×10^{-5} mol/L	Photocatalyst: 0.2 g/L; Light source: Xenon lamp; Irradiation time: 60 min	MB: 99.72% MO: 90.20%	[39]
Bi/$Bi_2O_2CO_3$	One-pot solvothermal	H_2 evolution	Photocatalyst: 0.5 g/L; Light source: Solar simulator; Irradiation time: 3 h	244.5 μmol/g	[60]
Bi@BiOCl	Solvothermal	RhB: 10 mg/L	Photocatalyst: 0.5 g/L; Light source: visible light; Irradiation time: 50 min	nearly 100%	[86]

metal@defective BiOCl by one-step solvothermal method. With 0.1 g of the prepared sample dispersed in the reaction system, NO removal ratio reached 67.5% after 30 min visible light irradiation. Dong *et al.* [97] fabricated Bi decorated BiOCl (Bi@BiOCl) by the reduction of partial Bi^{3+} to Bi, with the formation of oxygen vacancies. Under visible light irradiation, the photodegradation efficiency of NO was 50% for the optimal photocatalyst.

4. Bismuth single-atom in Bi/semiconductor composite

Since the pioneering work of Zhang *et al.* [98] who reported that the Pt_1/FeOx catalyst with anchoring single Pt atoms on the FeO_x support showed high activity for CO oxidation, single-atom catalysts (SACs) have become a novel and promising research topic in the field of heterogeneous catalysis. In general, a single-atom catalyst consists of the anchored isolated metal single-atoms and solid support [99]. The metal single-atoms can be stabilized by chemical interaction with the support or coordination with adjacent surface atoms [100]. Compared with metal clusters and nanoparticles, SACs generally exhibit excellent photocatalytic activity and selectivity [100]. This is mainly due to the following significant advantages of single-atom catalysts: (1) The increased active sites attributed to highly dispersed metal single-atoms [101,102], (2) the adsorption and activation of reactants promoted by unsaturated coordination environment [103], (3) enhanced light absorption and charge migration [104], (4) reduced catalysts cost ascribed to the maximum atom-utilization efficiency [100,103]. Therefore, single-atom catalysts in bismuth-based photocatalysts have also been reported in recent years.

Li *et al.* [105] reported a Bi single-atom modified TiO_2 nanosheet (TiO_2-Bi) catalyst prepared by a facile surface ion adsorption method for photocatalytic CO_2 reduction. The isolated bright spots

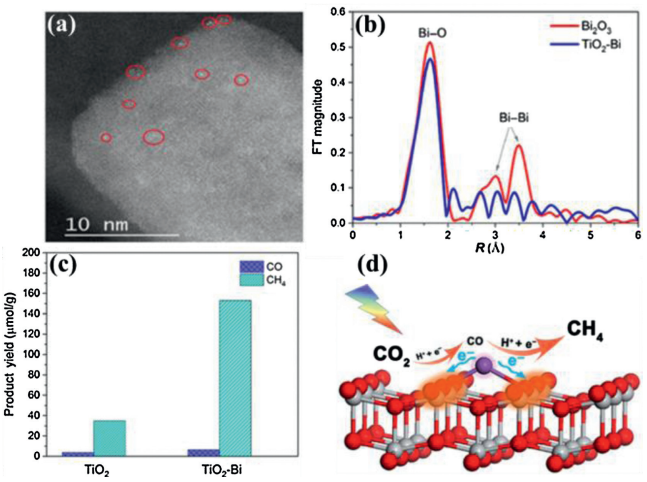

Fig. 4. (a) HAADF-STEM image of TiO_2-Bi sample. (b) EXAFS spectra of Bi L_3-edge in TiO_2-Bi and Bi_2O_3. (c) Comparison of photocatalytic CO_2 reduction performance of TiO_2-Bi and TiO_2. (d) Schematic of photocatalytic CO_2 reduction reaction over TiO_2-Bi. Reprinted with permission [105]. Copyright 2018, Springer.

on the TiO_2 nanosheets in the high-angle annular dark-field scanning transmission electron microscopy (HAADF-STEM) image were attributed to the single Bi atoms (Fig. 4a). According to the extended X-ray absorption fine structure (EXAFS) spectra (Fig. 4b), unlike Bi_2O_3, there is only one peak at 1.62 Å in the TiO_2-Bi sample, which corresponds to the Bi-O bond. In addition, the Bi-Bi bond in Bi_2O_3 was not observed in the TiO_2-Bi sample. These results indicated that Bi single-atom instead of Bi_2O_3 was generated on the TiO_2 nanosheets, and the isolated Bi atoms coordinated with O atoms on the surface of TiO_2. The lock-in based surface photovolage (SPV) test showed that the TiO_2-Bi sample possesses a stronger surface photovoltage response than TiO_2. This confirmed that the separation efficiency of photogenerated carriers was increased after the introduction of the Bi single-atom into TiO_2. The charge transfer mechanism was further explored through DFT calculations. The result of the charge density difference revealed that electrons transferred from the Bi single-atom to TiO_2, leading to charge redistribution on the surface of TiO_2. The built-in electric field in the TiO_2-Bi sample was induced, which accelerated the divorcement of photogenerated electrons and holes. Therefore, the TiO_2-Bi sample exhibited superior photocatalytic activity. In detail, the yield of CH_4 and CO on the TiO_2-Bi was 4.4 and 1.7 times than that over TiO_2 (Fig. 4c), respectively. The process of photocatalytic CO_2 reduction in this work is shown in Fig. 4d. In general, the efficient separation of photogenerated carriers due to the introduction of Bi single-atom mainly accounts for the enhancement of photocatalytic performance.

5. Conclusion and prospect

This review summarizes the development of metal Bi in photocatalysis in recent years. Bi can not only serve as a plasma photocatalyst, but also act as a cocatalyst to facilitate the efficient separation of photogenerated electron-hole pairs in the composite catalysts. Limited study on the application of Bi single atoms in photocatalysis has also been summarized. Although the studies on the role of Bi in the photocatalytic systems have achieved significant progress, a few research directions still deserve special attention.

(1) Basic mechanisms: The bismuth is easily oxidized to form thin bismuth oxide layer in the surrounding environment. Whether bismuth surface obtained by the available preparation methods contains bismuth oxides and how the bismuth oxide layers influence the photocatalytic process still remain unanswered. Some advanced characterization techniques (*e.g.*, EXAFS, X-ray absorption near-edge structure (XANES), HAADF-STEM, *in situ* XPS) need to be incorporated in future studies to improve the state of knowledge for photocatalytic reactions at the molecular or atomic level. Furthermore, *in situ* analytical techniques should be employed to monitor the variation of contaminants or catalysts during the reaction in real time. These technologies can help identify the intermediates generated during the reaction, thus allowing a reasonable inference of the reaction pathway.

(2) Development of Bi single atoms: Reducing nanoparticle size to single atoms can offer obvious advantages, such as reduced catalysts cost due to the maximum atom utilization rate and increased reactive sites. The studies on Bi nanoparticles has been extensively reported, which have laid the groundwork for further development of single atoms in a number of ways including the selection of preparation methods and supports. The stability and individual dispersion of atoms remain a challenge in the preparation of single-atom catalysts. Nowadays, single atoms catalysis has attracted growing attention in the field of catalysis. However, most studies related to single atoms focus on the development of noble metal single atoms. The studies on Bi single atoms catalysts are limited [106]. Therefore, the development of Bi single atoms deserves further studies.

(3) Explore Bi/semiconductors catalysts with strong reduction ability: The photocatalytic oxidation can mineralize antibiotics, dyes and other organic pollutants in the wastewater by hydroxyl radicals. The oxidative removal of some pollutants, such as NO, is not satisfactory. The final product of photocatalytic NO oxidation is NO_2^- and NO_3^-. These products accumulate on the surface of the catalysts during NO oxidation, leading to the deactivation of catalysts and second pollution in the environment. Therefore, it is desirable that Bi acts as a hole-capture center, coupled with a semiconductor possessing highly reductive CB electrons to convert NO to N_2 by photocatalytic reduction reaction. It is believed that the Bi/semiconductors with strong reduction ability have a promising application in the generation of clean energy, such as hydrogen production and CO_2 reduction.

Declaration of competing interest

The authors declare that they have no known competing financial interests or personal relationships that could have appeared to influence the work reported in this paper.

Acknowledgments

This work was financially supported by "Key Laboratory of Aerosol Chemistry and Physics, Institute of Earth Environment, CAS (No. KLACP1701)" and "State Key Laboratory of Loess and Quaternary Geology, Institute of Earth Environment, CAS (No. SKLLQG1516)".

Appendix A. Supplementary data

Supplementary material related to this article can be found, in the online version, at doi:https://doi.org/10.1016/j.cclet.2020.08.018.

References

[1] L. Hammarstrom, S. Hammes-Schiffer, Acc. Chem. Res. 42 (2009) 1859–1860.
[2] A. Fujishima, K. Honda, Nature 238 (1972) 37–39.

[3] N. Hao, Z. Xu, Y. Nie, et al., Chem. Eng. J. 378 (2019) 122222.
[4] Y. Rao, W. Chu, Y. Wang, Appl. Catal. A Gen. 468 (2013) 240–249.
[5] H. Ding, D. Han, Y. Han, et al., J. Hazard. Mater. 393 (2020) 122423.
[6] J. Wang, F. Han, Y. Rao, et al., Ind. Eng. Chem. Res. 57 (2018) 10226–10233.
[7] K. Hu, C. Chen, Y. Zhu, et al., J. Colloid Interface Sci. 540 (2019) 115–125.
[8] Y. Huang, P. Wang, Z. Wang, et al., Appl. Catal. B: Environ. 240 (2019) 122–131.
[9] X. Zhu, T. Zhang, Z. Sun, et al., Adv. Mater. 29 (2017) 1–7.
[10] T. Wang, D. Yue, X. Li, Y. Zhao, Appl. Catal. B: Environ. 268 (2020) 118399.
[11] F. Qin, H. Zhao, G. Li, et al., Nanoscale 6 (2014) 5402–5409.
[12] Z. Wang, Z. Chu, C. Dong, et al., ACS Appl. Nano Mater. 3 (2020) 1981–1991.
[13] J. Yang, T. Xie, Q. Zhu, et al., J. Mater. Chem. C 8 (2020) 2579–2588.
[14] A.U.R. Bacha, I. Nabi, Z. Fu, et al., Chin. Chem. Lett. 30 (2019) 2225–2230.
[15] M. Ji, Z. Zhang, J. Xia, et al., Chin. Chem. Lett. 29 (2018) 805–810.
[16] P. Li, Z. Zhou, Q. Wang, M. Guo, J. Am. Chem. Soc. 142 (2020) 12430–12439.
[17] Q. Chen, H. Long, M. Chen, et al., Appl. Catal. B: Environ. 272 (2020) 119008.
[18] Y. Ding, G. Zhang, X. Wang, L. Zhu, H. Tang, Appl. Catal. B: Environ. 202 (2017) 528–538.
[19] C. Li, G. Chen, J. Sun, et al., Appl. Catal. B: Environ. 188 (2016) 39–47.
[20] S. Obregon, A. Caballero, G. Colon, Appl. Catal. B: Environ. 117 (2012) 59–66.
[21] T. Tong, H. Zhang, J. Chen, D. Jin, J. Cheng, Catal. Comm. 87 (2016) 23–26.
[22] T. Wang, X. Liu, Q. Men, et al., Chin. J. Catal. 40 (2019) 886–894.
[23] X. Xu, L. Meng, Y. Dai, et al., J. Hazard. Mater. 381 (2020) 120953.
[24] J. Ding, Z. Dai, F. Qin, et al., Appl. Catal. B: Environ. 205 (2017) 281–291.
[25] J. Chen, J. Zhan, Y. Zhang, Y. Tang, Chin. Chem. Lett. 30 (2019) 735–738.
[26] Y. Bai, L. Ye, T. Chen, et al., Appl. Catal. B: Environ. 203 (2017) 633–640.
[27] X. Xu, X. Ding, X. Yang, et al., J. Hazard. Mater. 364 (2019) 691–699.
[28] L. Shi, J. Ma, L. Yao, L. Cui, W. Qi, J. Colloid Interface Sci. 519 (2018) 1–10.
[29] J. Wang, F. Han, Y. Rao, et al., Ind. Eng. Chem. Res. 57 (2018) 10226–10233.
[30] M. Li, H. Huang, S. Yu, N. Tian, Y. Zhang, ChemCatChem 10 (2018) 4477–4496.
[31] J. Xiong, P. Song, J. Di, H. Li, Z. Liu, J. Mater. Chem. A 7 (2019) 25203–25226.
[32] Z. Zhang, X. Sun, M. Dresselhaus, J. Ying, J. Heremans, Phys. Rev. B 61 (2000) 4850–4861.
[33] F. Dong, Q. Li, Y. Sun, W.K. Ho, ACS Catal. 4 (2014) 4341–4350.
[34] C. Liang, C.G. Niu, L. Zhang, et al., J. Hazard. Mater. 361 (2019) 245–258.
[35] J. Xiao, W. Yang, Q. Li, Appl. Catal. B: Environ. 218 (2017) 111–118.
[36] J. Wang, L. Tang, G. Zeng, et al., ACS Sustain. Chem. Eng. 5 (2017) 1062–1072.
[37] G. Jiang, X. Li, M. Lan, et al., Appl. Catal. B: Environ. 205 (2017) 532–540.
[38] Y. Li, S. Wang, Y. Zhao, J. Zhao, S. Bouasavanh, Colloids Surf. A 567 (2019) 112–120.
[39] J. Zhu, Y. Zhou, W. Wu, et al., J. Mater. Sci-Mater El. 31 (2020) 3845–3854.
[40] Z. Feng, D. Lian, X. Wu, et al., RSC Adv. 10 (2020) 2734–2739.
[41] Z. Gao, B. Yao, F. Yang, T. Xu, Y. He, Mater. Sci. Semicond. Process. 108 (2020) 104882.
[42] Q. Wang, H. Wu, Q. Gao, et al., J. Colloid Interface Sci. 548 (2019) 255–264.
[43] X. Xu, S. Kou, X. Guo, et al., J. Phys. Chem. C 121 (2017) 16257–16265.
[44] S. Yu, Y. Zhang, M. Li, X. Du, H. Huang, Appl. Surf. Sci. 391 (2017) 491–498.
[45] H. Zhou, S. Zhong, M. Shen, J. Hou, W. Chen, J. Alloys. Comp. 769 (2018) 301–310.
[46] M. Chen, Y. Li, Z. Wang, et al., Ind. Eng. Chem. Res. 56 (2017) 10251–10258.
[47] Y. Guo, S. Zhou, X. Sun, H. Yuan, Ceram. Int. 46 (2020) 14257–14261.
[48] M. Chen, X. Li, Y. Huang, et al., Appl. Surf. Sci. 513 (2020) 145775.
[49] X. Li, W. Zhang, W. Cui, et al., Appl. Catal. B: Environ. 221 (2018) 482–489.
[50] F. Dong, T. Xiong, Y. Sun, et al., Chem. Commun. 50 (2014) 10386–10389.
[51] J. Zhou, J. Gao, X. Xu, et al., J. Alloys. Comp. 709 (2017) 206–212.
[52] D. Zhang, Z. Xu, H. Zhao, et al., J. Mater. Sci. 55 (2020) 10765–10772.
[53] Z. Wang, S. Yan, Y. Sun, et al., Appl. Catal. B: Environ. 214 (2017) 148–157.
[54] Z. Ni, W. Zhang, G. Jiang, et al., Chin. J. Catal. 38 (2017) 1174–1183.
[55] K. Li, P. Chen, J. Li, et al., Catal. Sci. Technol. 8 (2018) 4600–4603.
[56] J. Xiao, W. Yang, Q. Li, Appl. Catal. B: Environ. 218 (2017) 111–118.
[57] K. Li, Y. Liang, J. Yang, et al., Catal. Sci. Technol. 9 (2019) 2543–2552.
[58] Z. Jiao, M. Shang, J. Liu, et al., Nano Energy 31 (2017) 96–104.
[59] W. He, Y. Sun, G. Jiang, et al., Appl. Catal. B: Environ. 232 (2018) 340–347.
[60] D. Sun, L. Huang, L. Li, et al., J. Colloid Interface Sci. 571 (2020) 80–89.
[61] K. Wang, Y. Li, G. Zhang, J. Li, X. Wu, Appl. Catal. B: Environ. 240 (2019) 39–49.
[62] J. Jia, P. Xue, R. Wang, et al., J. Chem. Technol. Biotechnol. 93 (2018) 2988–2999.
[63] X. Zhao, Z. Duan, L. Chen, Ind. Eng. Chem. Res. 58 (2019) 10402–10409.
[64] L. Zhang, C. Yang, K. Lv, et al., Chin. J. Catal. 40 (2019) 755–764.
[65] H. Ma, Y. Zhao, B. Souvanhthong, J. Zhao, J. Colloid Interface Sci. 531 (2018) 311–319.
[66] F. Deng, Q. Zhang, L. Yang, et al., Appl. Catal. B: Environ. 238 (2018) 61–69.
[67] J. Pan, J. Liu, H. Ma, et al., New J. Chem. 42 (2018) 7293–7300.
[68] D. Chen, S. Wu, J. Fang, et al., Sep. Purif. Technol. 193 (2018) 232–241.
[69] J. Yin, Z. Xing, J. Kuang, et al., J. Alloys. Comp. 750 (2018) 659–668.
[70] J. Lv, J. Zhang, J. Liu, et al., ACS Sustain. Chem. Eng. 6 (2017) 696–706.
[71] F. Yang, X. Zhu, J. Fang, et al., Ceram. Int. 44 (2018) 6918–6925.
[72] M. Du, S. Zhang, Z. Xing, et al., Langmuir 35 (2019) 7887–7895.
[73] X. Xu, N. Yang, P. Wang, et al., ACS Appl. Mater. Interfaces 12 (2020) 1867–1876.
[74] J. Li, Xa. Dong, Y. Sun, W. Cen, F. Dong, Appl. Catal. B: Environ. 226 (2018) 269–277.
[75] X. Liu, X. Xiong, S. Ding, Q. Jiang, J. Hu, Catal. Sci. Technol. 7 (2017) 3580–3590.
[76] S. Luo, J. Xu, Z. Li, et al., Nanoscale 9 (2017) 15484–15493.
[77] H. Xu, Y. Hu, D. Huang, et al., ACS Sustain. Chem. Eng. 7 (2019) 5784–5791.
[78] D. Zhang, H. Liu, C. Su, H. Li, Y. Geng, Sep. Purif. Technol. 218 (2019) 1–7.
[79] F. Chang, B. Lei, X. Zhang, et al., Colloids Surf. A 572 (2019) 290–298.
[80] U.A. Khan, J. Liu, J. Pan, et al., Appl. Surf. Sci. 484 (2019) 341–353.
[81] H. Liu, H. Zhou, X. Liu, et al., J. Alloys Comp. 798 (2019) 741–749.
[82] Y. Huang, H. Xu, D. Luo, et al., J. Alloys Comp. 806 (2019) 418–427.
[83] X. Li, Y. Sun, T. Xiong, et al., J. Catal. 352 (2017) 102–112.
[84] Y. Cheng, N.H. Shah, J. Yang, et al., ACS Appl. Nano Mater. 2 (2019) 6418–6427.
[85] L. Xu, W.-q. Chen, S.-q. Ke, et al., Chem. Eng. J. 382 (2020) 122810.
[86] X. Su, L. Hou, L. Xia, et al., J. Mater. Sci. 54 (2018) 4559–4572.
[87] X. Li, W. Zhang, J. Li, et al., Appl. Catal. B: Environ. 241 (2019) 187–195.
[88] W. He, Y. Sun, G. Jiang, et al., Appl. Catal. B: Environ. 239 (2018) 619–627.
[89] X. Li, W. Zhang, W. Cui, et al., Chem. Eng. J. 370 (2019) 1366–1375.
[90] M. Sun, X. Dong, B. Lei, et al., Nanoscale 11 (2019) 20562–20570.
[91] X. Yang, S. Wang, N. Yang, et al., Appl. Catal. B: Environ. 259 (2019) 118088.
[92] M. Ran, H. Wang, W. Cui, et al., ACS Appl. Mater. Interfaces 11 (2019) 47984–47991.
[93] P. Chen, H. Liu, Y. Sun, et al., Appl. Catal. B: Environ. 264 (2020) 118545.
[94] Z. Cui, X. Dong, Y. Sun, et al., Nanoscale 10 (2018) 16928–16934.
[95] X. Dong, W. Zhang, Y. Sun, et al., J. Catal. 357 (2018) 41–50.
[96] H. Wang, W. Zhang, X. Li, et al., Appl. Catal. B: Environ. 225 (2018) 218–227.
[97] F. Dong, T. Xiong, S. Yan, et al., J. Catal. 344 (2016) 401–410.
[98] B. Qiao, A. Wang, X. Yang, et al., Nat. Chem. 3 (2011) 634–641.
[99] Q. Wang, D. Zhang, Y. Chen, W. Fu, X. Lv, ACS Sustain. Chem. Eng. 7 (2019) 6430–6443.
[100] C. Gao, J. Low, R. Long, et al., Chem. Rev. (2020) doi:10.1021/acs.chemrev.9b00840
[101] A. Alarawi, V. Ramalingam, J.H. He, Mater. Today Energy 11 (2019) 1–23.
[102] S. Hejazi, S. Mohajernia, B. Osuagwu, et al., Adv. Mater. 32 (2020) e1908505.
[103] B. Wang, H. Cai, S. Shen, Small Methods 3 (2019) 1800447.
[104] Q. Wang, J. Li, X. Tu, et al., Chem. Mater. 32 (2019) 734–743.
[105] X. Li, W. Bi, Z. Wang, et al., Nano Res. 11 (2018) 3362–3370.
[106] E. Zhang, T. Wang, K. Yu, et al., J. Am. Chem. Soc. 141 (2019) 16569–16573.